Observation of new neutron-rich Mn, Fe, Co, Ni, and Cu isotopes in the vicinity of ^{78}Ni

T. Sumikama,[1,2,*] S. Nishimura,[2] H. Baba,[2] F. Browne,[3,2] P. Doornenbal,[2] N. Fukuda,[2] S. Franchoo,[4] G. Gey,[5,2,6] N. Inabe,[2] T. Isobe,[2] P. R. John,[7,8] H. S. Jung,[9] D. Kameda,[2] T. Kubo,[2] Z. Li,[10] G. Lorusso,[2] I. Matea,[4] K. Matsui,[11] P. Morfouace,[4] D. Mengoni,[12] D. R. Napoli,[13] M. Niikura,[11] H. Nishibata,[14] A. Odahara,[14] E. Sahin,[15] H. Sakurai,[2,11] P.-A. Söderström,[2] G. I. Stefan,[4] D. Suzuki,[4,2] H. Suzuki,[2] H. Takeda,[2] R. Taniuchi,[11] J. Taprogge,[16,17,2] Zs. Vajta,[18,2] H. Watanabe,[19] V. Werner,[20] J. Wu,[10,2] Z. Y. Xu,[11] A. Yagi,[14] and K. Yoshinaga[21,2]

[1]*Department of Physics, Tohoku University, 6-3 Aramaki-Aoba, Aoba, Sendai 980-8578, Japan*
[2]*RIKEN Nishina Center, 2-1 Hirosawa, Wako, Saitama 351-0198, Japan*
[3]*School of Computing, Engineering and Mathematics, University of Brighton, Brighton, BN2 4GJ, United Kingdom*
[4]*Institut de Physique Nucléaire, CNRS-IN2P3, Université Paris-Sud, Université Paris-Saclay, 91406 Orsay Cedex, France*
[5]*LPSC, Université Joseph Fourier Grenoble 1, CNRS/IN2P3, Institut National Polytechnique de Grenoble, F-38026 Grenoble Cedex, France*
[6]*ILL, 38042 Grenoble Cedex, France*
[7]*Dipartimento di Fisica e Astronomia, Università di Padova, I-35131 Padova, Italy*
[8]*Istituto Nazionale di Fisica Nucleare, Sezione di Padova, I-35131 Padova, Italy*
[9]*Department of Physics, University of Notre Dame, Notre Dame, Indiana 46556, USA*
[10]*Department of Physics, Peking University, Beijing 100871, China*
[11]*Department of Physics, University of Tokyo, 7-3-1 Hongo, Bunkyo, Tokyo 113-0033, Japan*
[12]*Dipartimento di Fisica, Universita di Padova, I-35131 Padova, Italy*
[13]*Institute Nazionale di Fisica Nucleare, Laboratori Nazionali di Legnaro, I-35020 Legnaro, Italy*
[14]*Department of Physics, Osaka University, 1-1 Machikaneyama, Toyonaka, Osaka 560-0043, Japan*
[15]*Department of Physics, University of Oslo, Oslo, Norway*
[16]*Departamento de Física Teórica, Universidad Autónoma de Madrid, E-28049 Madrid, Spain*
[17]*Instituto de Estructura de la Materia, CSIC, E-28006 Madrid, Spain*
[18]*MTA Atomki, P.O. Box 51, Debrecen H-4001, Hungary*
[19]*International Research Center for Nuclei and Particles in the Cosmos, Beihang University, Beijing 100191, China*
[20]*Wright Nuclear Structure Laboratory, Yale University, New Haven, Connecticut 06520-8120, USA*
[21]*Department of Physics, Tokyo University of Science, 2641 Yamazaki, Noda, Chiba 278-8510, Japan*

Neutron-rich nuclei in the vicinity of ^{78}Ni were produced using a ^{238}U beam at the RIKEN Radioactive Isotope Beam Factory. The particle-identification plot for the in-flight fission fragments highlights the first observation of eight new isotopes: ^{73}Mn, ^{76}Fe, ^{77,78}Co, ^{80,81,82}Ni, and ^{83}Cu. Although the β-decay half-lives of ^{77}Co and ^{80}Ni were recently reported by Xu *et al.* [Phys. Rev. Lett. **113**, 032505 (2014)] using data from the same experiment, the current work provides the first direct, quantitative evidence for the existence of these isotopes. The experimental production cross sections are reproduced in a satisfactory manner by theoretical predictions. An odd-even staggering of the cross sections was observed, and the effect appears to become more pronounced for the most exotic nuclei that were investigated. The staggering effect was interpreted as an increase of the neutron-evaporation probability for odd-N isotopes, owing to the decrease of the neutron-separation energy, S_n. The predicted cross section for ^{80}Ni is significantly overestimated, which may be related to a weak binding of the neutron pair above the $N = 50$ shell closure.

The shell structure of the atomic nucleus plays an important role in many aspects of nuclear physics. Around the line of β stability, the nuclear magic numbers have been firmly established as 2, 8, 20, 28, 50, and 82 [1–3]. However, far from stability, the disappearance of certain magic numbers have been reported; for example, the neutron magic numbers $N = 8$, 20, and 28 are known to weaken in exotic systems [4–10]. The neutron-rich nucleus ^{78}Ni, which lies close on the Segre chart to the nuclei investigated in the present work, contains the traditional nuclear magic numbers $Z = 28$ and $N = 50$. Indeed, the neutron number $N = 50$ has attracted a lot of attention regarding the robustness of this magic number in exotic nuclei. The experimental $N = 50$ shell gap energy, Δ_{2n}, has been measured as far down as Zn ($Z = 30$) isotopes for $\Delta_{2n} = S_{2n}(N = 50) - S_{2n}(N = 52)$, where S_{2n} is the two-neutron separation energy. The quantity decreases from $Z = 40$ to $Z = 32$ and then increases slightly to $\Delta_{2n} = 3.5$ MeV at $Z = 30$ [11,12]. Moreover, a recent spectroscopic study on ^{80}Zn suggests that the two-proton configuration can be described as a ^{78}Ni core with a robust $N = 50$ shell closure [13].

The structures of the even-even Ni isotopes up to ^{76}Ni [14] and the shortening of β-decay half-lives of Co ($Z = 27$) isotopes relative to Ni isotopes up to $N = 50$ [15] provide

*sumikama@ribf.riken.jp

experimental evidence for the robust nature of the $Z = 28$ shell closure. The experimental $Z = 28$ shell gap energy, Δ_{2p}, has been determined up to $N = 42$, where $\Delta_{2p} = S_{2p}(Z = 28) - S_{2p}(Z = 30)$, and S_{2p} is the two-proton separation energy [11]. Studies on the Co, Ni, and Cu isotopes indicate that the $Z = 28$ shell gap at $N \geqslant 44$, which is formed between the proton $f_{7/2}$ and $f_{5/2}$ orbits, decreases towards $N = 50$ as interpreted by the monopole effect of the tensor force between the proton $f_{7/2}$ or $f_{5/2}$, and neutron $g_{9/2}$ orbits [16–18].

The first step toward studies on and beyond ^{78}Ni involves the production of new isotopes in this exotic region [19]. In the present work, new isotopes in the vicinity of ^{78}Ni were investigated at the RIKEN Radioactive Isotope Beam Factory (RIBF) using a primary beam of ^{238}U ions with an average intensity of 6.84 pnA. Here, we report on the first observation of eight isotopes, namely, ^{73}Mn, ^{76}Fe, ^{77,78}Co, ^{80,81,82}Ni, and ^{83}Cu, and the production cross sections of Mn, Fe, Co, Ni, and Co isotopes. In addition to the results reported in the present work, the radioactive ion (RI) beam was also used for β-decay spectroscopic studies to investigate the shell structure and β-decay properties of ^{78}Ni and its neighbors during an EURICA campaign [15,20,21]; note that the β-decay half lives of ^{77}Co and ^{80}Ni, two of the isotopes reported in the present work, were deduced using data from the same experiment [15]. However, it is stressed that the rejection of background events in the particle identification (PID) has been improved in the present study, and significance tests (discussed below) were performed in order to provide the first direct evidence of new isotopes in the PID.

The RI beams were produced via in-flight fission of a ^{238}U primary beam at 345 MeV/nucleon on a 3-mm-thick beryllium target. The fission fragments were transported to the BigRIPS separator and ZeroDegree spectrometer [22,23] for analysis. Two wedge-shaped energy degraders were placed at the dispersive focal planes F1 and F5 for the purification of the RI beams. The location of each focal plane is indicated in Fig. 1 of Ref. [23]. The thicknesses of the degraders at F1 and F5 were 5.94 and 4.43 mm, respectively. The experimental conditions are summarized in Table I for five settings, which are labeled as A, B, C, D, and E.

For the identification of the RI beam constituents, energy losses (ΔE), times of flight (TOF), and magnetic rigidities ($B\rho$) were measured on an event-by-event basis: TOF was measured using two plastic scintillator detectors placed at F3 and F7, each with a thickness of 200 μm; $B\rho$ values were deduced from trajectory reconstructions using position and angle measurements at the F3, F5, and F7 focal planes with position-sensitive parallel-plate avalanche counters (PPACs) [24]; and ΔE was measured using a multisampling ionization chamber (MUSIC) [25] placed at F11. Details on the production of the PID are described in Ref. [26].

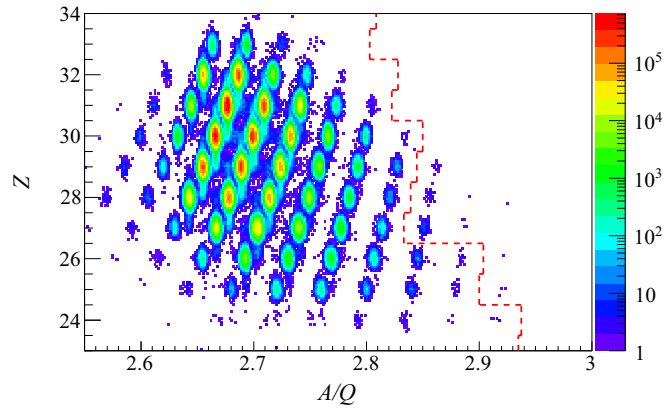

FIG. 1. Particle-identification plot for isotopes measured in the present work (see text for details); the atomic number, Z, vs the mass-to-charge ratio, A/Q, is displayed. The red dashed line indicates the boundary of the isotopes previously reported [19,27].

The PID plot deduced in the present work, which was obtained from the sum of all settings, is provided in Fig. 1. Because the magnetic rigidity of setting E was slightly different from the others, different parameters in the analysis were used. The relative resolution of the mass-to-charge ratio, A/Q, was 0.06% (1σ) and the absolute resolution of Z was 0.14 (1σ) for ^{78}Ni.

It is possible that the atomic number of an ion can change after the A/Q measurement between F3 and F7, and before the Z measurement by the MUSIC detector at F11, owing to secondary reactions in detectors located at F7 and F11, the exit window of the F11 chamber, the entrance window of the MUSIC detector, and the air between the two windows. The

TABLE I. Summary of the experimental conditions for the five settings discussed in the text. The magnetic rigidities, $B\rho$, of the dipole magnets in BigRIPS [22,23] are shown. Note that the positive directions of the slits are on the right-hand sides, as viewed from the downstream direction. Slits that were fully opened are not provided here.

Setting	A	B	C	D	E
Bρ of D1 (Tm)	8.2450	8.2450	8.2450	8.2450	8.2440
Bρ of D2 (Tm)	7.6540	7.6540	7.6540	7.6540	7.6460
Bρ of D3 and D4 (Tm)	7.5715	7.5715	7.5715	7.5715	7.6460
Bρ of D5 and D6 (Tm)	7.0675	7.0675	7.0675	7.0675	7.1545
F1 slit (mm)	−64.2/+44.0	−64.2/+44.0	−64.2/+44.0	−64.2/+40.0	−64.2/+42.8
F2 slit (mm)	−14.0/+14.0	−14.0/+17.0	−14.0/+17.0	−14.0/+23.0	−14.0/+17.0
F5 slit (mm)	−120.0/+120.0	−120.0/+120.0	−120.0/+120.0	−120.0/+120.0	−120.0/+120.0
F7 slit (mm)	−50.0/+50.0	−50.0/+50.0	−20.0/+25.0	−20.0/+25.0	−50.0/+50.0
Irradiation time (h)	8.7	5.5	120.3	12.5	128.7
Beam dose (particles)	5.40×10^{14}	7.12×10^{14}	1.48×10^{16}	1.20×10^{15}	2.36×10^{16}

total thickness of the materials listed above was 90 mg/cm^2, and there were no detectors at the F8, F9, or F10 foci during the present experiment. The secondary-reaction events were rejected as follows. The two $B\rho$ values between F3 and F5 ($B\rho_{35}$) and between F5 and F7 ($B\rho_{57}$) were measured; the change in $B\rho$ due to the energy loss of an ion in the F5 degrader is defined by $\Delta(B\rho/B\rho_c) = B\rho_{35}/B\rho_{35c} - B\rho_{57}/B\rho_{57c}$, where $B\rho_{35c}$ and $B\rho_{57c}$ are the central $B\rho_{35}$ and $B\rho_{57}$ values, respectively. At typical RIBF beam energies, $\Delta(B\rho/B\rho_c)$ roughly depends on the neutron number. Thus, $\Delta(B\rho/B\rho_c)$ and A/Q together provide additional information on Z between F3 and F7, and the unreacted events should have a consistent correlation among Z, A/Q, and $\Delta(B\rho/B\rho_c)$. This correlation was used to reject events resulting from secondary reactions. Note that the distribution of each isotope in Fig. 1 has a short tail component in the Z direction because the techniques discussed above do not work effectively when $\Delta Z = 1$.

Figure 2 provides A/Q projections that were produced from Fig. 1 with gates defined by $Z \pm 0.3$ for the Cr, Mn, Fe, Co, Ni, and Cu isotopic chains. For the new isotope candidates ^{73}Mn, ^{76}Fe, ^{77,78}Co, ^{80,81,82}Ni, and ^{83}Cu, significance tests using p values were performed as described in Ref. [19]. Each p value, which is the probability of misidentifying all the measured events, was obtained by taking into account contamination from hydrogen-like ions ($Q = Z - 1$), secondary reactions, and random background events.

Following their transportation from F3 to F5, most of the hydrogen-like ions became fully stripped in the thick F5 degrader due to the charge-stripping process, and were removed from the beam using hardware slits at F7. Therefore, the contribution of hydrogen-like ions in the PID plot is negligible. The upper limit on the ratio of hydrogen-like to fully stripped ions was evaluated for ^{83}Ga. The ratio between the number of ^{83}Ga^{30+} and ^{83}Ga^{31+} was deduced to be less than 1.8×10^{-6}. The upper limit for nuclei with $Z < 31$ could not be determined more precisely than for ^{83}Ga; however, the upper limit for ^{83}Ga can be adopted for $Z < 31$ because the ratio decreases with Z.

The arrows in Fig. 2 indicate the contaminants produced in the secondary-reaction events discussed above. These are reacted events from $^{A-3}(Z-1)$ and $^{A+3}(Z+1)$ around ^{A}Z in the A/Q projection. The number of reacted events is proportional to the yield of $^{A-3}(Z-1)$ and $^{A+3}(Z+1)$, respectively. The ratio of the reacted events to the yield was determined for all of the isotopes. The averaged ratios, 0.055% for $^{A-3}(Z-1)$ and 0.073% for $^{A+3}(Z+1)$, were used in the p-value evaluations.

Other sources of background for a given isotope ^{A}Z were found to be caused mainly by ^{A-1}Z events, by comparing the position distribution at each focal plane, the momentum distribution, ΔE, and detector responses between the background and properly identified events. The background level was evaluated for ^{77}Ni; the contamination arising from ^{76}Ni was estimated using the background between ^{76}Ni and ^{77}Ni. The number of background events was obtained using the number of counts in the range $A/Q = 2.73$ to 2.738 in Fig. 2, which corresponds to $\pm 2.4\sigma_{A/Q}$. The ratio of the background at ^{77}Ni and the yield of ^{76}Ni was obtained to be 4×10^{-5}, and this value was employed to estimate the background contribution in the evaluation of the p value.

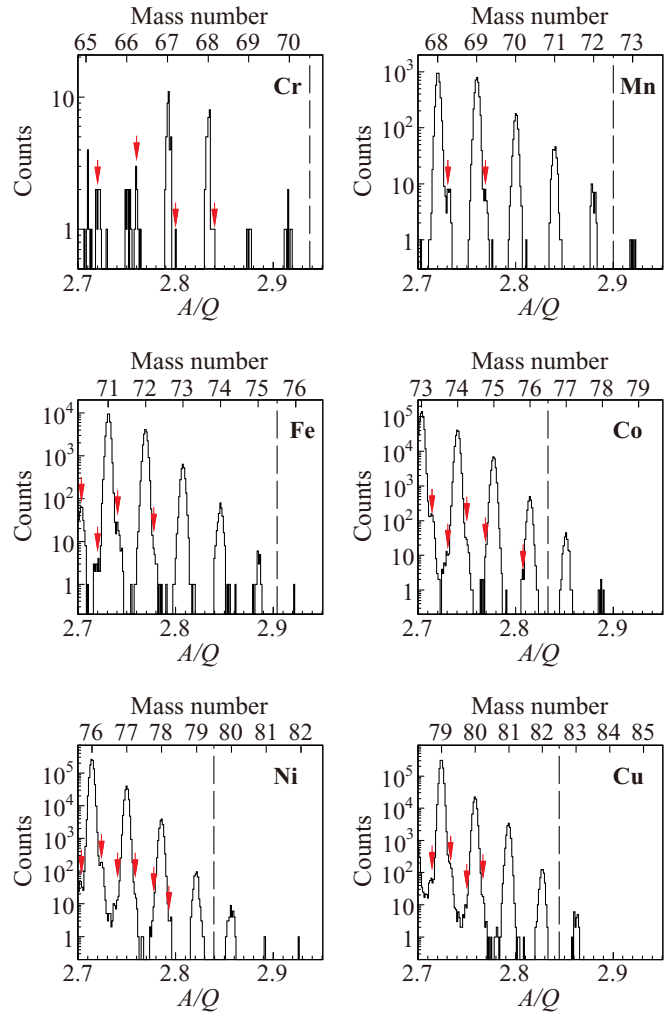

FIG. 2. A/Q projections for the Cr, Mn, Fe, Co, Ni, and Cu isotopic chains. The dashed lines indicate the boundaries between the isotopes previously reported [19,27] and the new results. The red arrows indicate contaminants resulting from reactions that occur after the A/Q measurements and before the Z measurements. Only the relatively strong contaminants are highlighted.

The p values of ^{73}Mn, ^{76}Fe, ^{77,78}Co, ^{80,81,82}Ni, and ^{83}Cu, which are summarized in Table II, are all less than 1%, providing the first direct, quantitative evidence for the existence of these isotopes. Owing to the fact that only one event was observed for each of ^{76}Fe, ^{81}Ni, and ^{82}Ni, further confirmation for these isotopes was acquired. Specifically, the ion trajectories at F3, F5, F7, and F11, in addition to detector responses, were compared to those of lighter isotopes. For example, the F3 horizontal position of ^{82}Ni was compared as follows: Since the F3 position of Ni isotopes depends on the mass number, the expected position of ^{82}Ni was determined to be -16.3 mm from the extrapolations of lighter Ni isotopes. The standard deviation, σ_x, of the distribution was 3.5 mm on average and, therefore, the measured position of -15.3 mm lies within $1\sigma_x$ of the expected position.

TABLE II. Number of counts, p values, and production cross sections, σ, for new isotopes identified in the present work.

Nuclide	Count	p value (%)	σ (mb)
^{73}Mn	3	<0.01	$(1.4^{+1.4}_{-0.8}) \times 10^{-11}$
^{76}Fe	1	0.27	$(4^{+10}_{-3}) \times 10^{-12}$
^{77}Co	178	<0.01	$(1.22 \pm 0.15) \times 10^{-9}$
^{78}Co	5	<0.01	$(2.5^{+1.7}_{-1.1}) \times 10^{-11}$
^{80}Ni	36	<0.01	$(2.3^{+0.5}_{-0.4}) \times 10^{-10}$
^{81}Ni	1	0.35	$(5^{+11}_{-4}) \times 10^{-12}$
^{82}Ni	1	0.10	$(6^{+14}_{-5}) \times 10^{-12}$
^{83}Cu	21	<0.01	$(1.7^{+0.5}_{-0.4}) \times 10^{-10}$

The production cross sections, listed in Table II, were deduced using data from settings C and E; for each setting, data were acquired over a relatively long irradiation time and used to check whether a new isotope is consistent with systematic trends. The transmission efficiencies and losses due to secondary reactions in the beam line detectors and other materials were taken into account. These were determined using experimental data and simulations. The transmission losses at the slits placed at the achromatic focal planes F2 and F7 were deduced from experimental data. The transmission losses at the slits of the momentum dispersive focal planes F1 and F5, and the angular acceptances of BigRIPS, were simulated using the Monte Carlo mode of the LISE++ program (version 9.7.3) [28]. Systematic uncertainties on momentum distributions and corresponding acceptances were estimated by changing the momentum dispersions within ±10%. The reaction losses within the target, F7 detectors, and detectors downstream of F7 were estimated using LISE++ and experimental data.

The production cross sections, σ, are presented as a function of neutron number in Fig. 3 alongside predictions

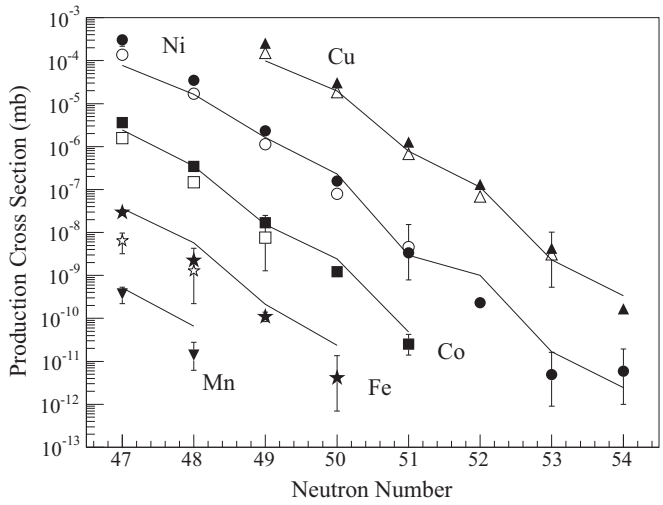

FIG. 3. Production cross sections for Mn, Fe, Co, Ni, and Cu isotopes. The filled and open markers are present and previous [19] results, respectively. The lines indicate predictions by the LISE++ program (version 8.4.1) [28].

of the abrasion-fission model implemented in LISE++. The parameters used in the model were same as those adopted in Ref. [29], where the predictions were compared to a large number of measured cross sections from $Z = 20$ to 54. The cross sections measured in the present work for ^{73}Mn, ^{76}Fe, ^{77,78}Co, ^{80,81}Ni, and ^{83}Cu change smoothly as a function of proton and neutron numbers. It is noted that although the experimental cross sections for ^{82}Ni and ^{81}Ni are consistent owing to their relatively large uncertainties, the predictions suggest that the cross section of ^{82}Ni is approximately one order of magnitude smaller than ^{81}Ni, as is the case of ^{80}Ni and ^{79}Ni, where $\sigma(^{80}\text{Ni})/\sigma(^{79}\text{Ni}) = 7\%$. Because the 1σ interval of the Poisson distribution for a single event is from 0.17 to 3.3, a single event for each of ^{81}Ni and ^{82}Ni is in fact consistent with the expected decrease of the cross section.

The cross sections reported in Ref. [19] are also displayed in Fig. 3. Although the cross sections measured in the present work relative to the cross section of ^{78}Ni are consistent with the previous values [19], the absolute cross sections reported here are about twice as large as those in Ref. [19]. The primary beam intensity was monitored by measuring light charged particles scattered from the production target using three plastic scintillation counters for both experiments. The calibration methods, however, were different. In the previous study [19], the beam current as a reference was measured by a Faraday cup placed at the beginning of the transport line from the accelerator complex to the production target, because a Faraday cup placed at the chamber of the production target could not be used due to an insufficient electron suppression of the Faraday cup. However, the transport efficiency from the accelerator to the production target became ambiguous. To resolve this ambiguity, the calibration method was improved in the present study. The number of $^{238}U^{87+}$ after the production target and the number of scattered particles were measured simultaneously prior to the measurements reported here. The charge-state distribution of ^{238}U after the production target was also measured to determine the ratio of $^{238}U^{87+}$ and the sum of all the charge states. From these measurements, the ratio between the number of scattered particles and the primary-beam intensity was determined. Because the calibration was based on the direct measurement of the primary beam, the present results are more accurate.

As shown in Fig. 3, an odd-even staggering of the cross sections as a function of neutron number is predicted; such behavior was confirmed by the present work, particularly toward the largest neutron numbers investigated here. For example, while the ratio of the cross sections between ^{78}Ni and ^{77}Ni is $\sigma(^{78}\text{Ni})/\sigma(^{77}\text{Ni}) = 1/15$, the ratio between ^{79}Ni and ^{78}Ni is $\sigma(^{79}\text{Ni})/\sigma(^{78}\text{Ni}) = 1/47$. The predicted ratios also highlight the staggering as $\sigma(^{78}\text{Ni})/\sigma(^{77}\text{Ni}) = 1/7$ and $\sigma(^{79}\text{Ni})/\sigma(^{78}\text{Ni}) = 1/78$; however, the difference between two ratios is larger than the experimental result.

Because of the paring energy, it is expected that for odd-N nuclei the reaction Q value decreases and the neutron-evaporation probability increases as a result of the lowering of the neutron-separation energy, S_n. Both of these characteristic features decrease the cross section. The cross section without particle evaporation was calculated for ^{77,78,79}Ni to understand the effect of neutron evaporation, which is generally

significant for very neutron-rich nuclei. The predicted ratios without particle evaporation suggest a much smaller staggering: $\sigma(^{78}\mathrm{Ni})/\sigma(^{77}\mathrm{Ni}) = 1/4.7$ and $\sigma(^{79}\mathrm{Ni})/\sigma(^{78}\mathrm{Ni}) = 1/5.5$. Therefore, the observed odd-even staggering in σ can be interpreted mainly as a result of the large neutron-evaporation probability. In the calculation, $S_n(^{79}\mathrm{Ni}) = 0.72$ MeV was adopted; its low value is affected by the $N = 50$ shell gap and is slightly lower than but consistent with the evaluated value of 1.75 ± 0.85 MeV in the atomic mass evaluation (AME2016) [11]. The level schemes of the $N = 51$ isotones ^{83}Ge and ^{85}Se contain only one excited state each below 1 MeV [30,31]. Because the number of states below S_n is also expected to be low for ^{79}Ni, the large probability of the neutron evaporation is probable. The odd-even staggering for other cases could also be interpreted by the lowering of S_n in odd-N isotopes, because a similar effect is expected far from the valley of stability.

Finally, it is noted that the cross section of ^{80}Ni is significantly overestimated: The predicted value is 4.3 times as large as the measured one. If it is due to a large neutron evaporation probability, the two neutrons above $N = 50$ in ^{80}Ni might be less bound than the prediction suggests, where a mass excess of -22.8 MeV was assumed.

In summary, neutron-rich nuclei in the vicinity of ^{78}Ni were produced using the in-flight fission reaction with an intense ^{238}U beam on a beryllium production target. The fission fragments were purified by the BigRIPS separator, and particle identification was performed on an event-by-event basis by measuring projectile times of flight, magnetic rigidities, and energy losses in an ionization chamber. Significance tests were performed by estimating contaminant quantities and provide the first direct, quantitative evidence for the existence of ^{73}Mn, ^{76}Fe, ^{77,78}Co, ^{80,81,82}Ni, and ^{83}Cu. The production cross sections along the respective isotopic chains were reproduced in a satisfactory manner by predictions of the LISE++ program, including the results for the new isotopes reported here. Odd-even staggerings of the production cross sections were observed, and the effect appears to become more pronounced for the most exotic nuclei investigated. The staggering among ^{77,78,79}Ni can be understood using predictions of production cross sections with and without particle evaporation after abrasion fission at the production target. The large decrease in the cross section between ^{78}Ni and ^{79}Ni was interpreted mainly as a result of the large evaporation probability of neutron above the $N = 50$ shell for ^{79}Ni. It is noted that the cross section of ^{80}Ni is largely overestimated. If the discrepancy is due to neutron evaporation, it may indicate that the two neutrons above the $N = 50$ magic number are less bound than current estimates suggest. For further insight, the masses of the isotopes investigated in the present work are required. Indeed, when these masses are known, the measured regions about the $N = 50$ and $Z = 28$ shell gaps can be extended down to $Z = 28$ and up to $N = 50$, respectively, i.e., the doubly magic nucleus ^{78}Ni. Significant experimental input is expected in the future, especially for measurements of the $Z = 28$ shell gap, which is currently known up to $N = 42$. The rare-RI ring, which was recently constructed at RIBF to serve as a RI-beam storage ring, will be a key device for mass measurements of very rare isotopes [32].

The authors acknowledge the accelerator staff for their efforts in delivering an intense and stable ^{238}U beam. T.S. is grateful to Dr. D. Steppenbeck for proofreading the paper. This work was supported by JSPS KAKENHI (25247045, 25800130), the Spanish Ministerio de Ciencia e Innovación under Contracts No. FPA2009-13377-C02 and No. FPA2011-29854-C04, OTKA Contract No. K-100835, U.S. DOE Contract No. DE-FG02-91ER40609, and the Priority Centers Research Program in Korea (2009-0093817).

[1] W. M. Elsasser, J. Phys. Radium **5**, 635 (1934).
[2] M. Goeppert-Mayer, Phys. Rev. **75**, 1969 (1949).
[3] O. Haxel, J. H. D. Jensen, and H. E. Suess, Phys. Rev. **75**, 1766 (1949).
[4] C. Détraz *et al.*, Phys. Rev. C **19**, 164 (1979).
[5] D. Guillemaud-Mueller *et al.*, Nucl. Phys. A **426**, 37 (1984),
[6] T. Motobayashi *et al.*, Phys. Lett. B **346**, 9 (1995).
[7] A. Navin *et al.*, Phys. Rev. Lett. **85**, 266 (2000).
[8] H. Iwasaki *et al.*, Phys. Lett. B **481**, 7 (2000).
[9] B. Bastin *et al.*, Phys. Rev. Lett. **99**, 022503 (2007).
[10] S. Takeuchi *et al.*, Phys. Rev. Lett. **109**, 182501 (2012).
[11] W. J. Huang *et al.*, Chin. Phys. C **41**, 030002 (2017); M. Wang *et al.*, *ibid.* **41**, 030003 (2017).
[12] R. N. Wolf *et al.*, Phys. Rev. Lett. **110**, 041101 (2013).
[13] Y. Shiga *et al.*, Phys. Rev. C **93**, 024320 (2016); **93**, 049904(E) (2016).
[14] C. Mazzocchi *et al.*, Phys. Lett. B **622**, 45 (2005).
[15] Z. Y. Xu *et al.*, Phys. Rev. Lett. **113**, 032505 (2014).
[16] O. Sorlin and M.-G. Porquet, Prog. Part. Nucl. Phys. **61**, 602 (2008).
[17] T. Otsuka, T. Suzuki, R. Fujimoto, H. Grawe, and Y. Akaishi, Phys. Rev. Lett. **95**, 232502 (2005).
[18] K. Sieja and F. Nowacki, Phys. Rev. C **81**, 061303(R) (2010).
[19] T. Ohnishi *et al.*, J. Phys. Soc. Jpn. **79**, 073201 (2010).
[20] S. Nishimura, Prog. Theor. Exp. Phys. **2012**, 03C006 (2012).
[21] P.-A. Söderström *et al.*, Phys. Rev. C **92**, 051305(R) (2015).
[22] T. Kubo, Nucl. Instrum. Meth. B **204**, 97 (2003).
[23] T. Kubo *et al.*, Prog. Theor. Exp. Phys. **2012**, 03C003 (2012).
[24] H. Kumagai *et al.*, Nucl. Instrum. Meth. B **317**, 717 (2013).
[25] Y. Sato *et al.*, Jpn. J. Appl. Phys. **53**, 016401 (2014).
[26] N. Fukuda *et al.*, Nucl. Instrum. Meth. B **317**, 323 (2013).
[27] O. B. Tarasov *et al.*, Phys. Rev. C **87**, 054612 (2013).
[28] O. B. Tarasov and D. Bazin, Nucl. Instrum. Meth. B **266**, 4657 (2008).
[29] H. Suzuki *et al.*, Nucl. Instrum. Meth. B **317**, 756 (2013).
[30] K. Kolos *et al.*, Phys. Rev. C **88**, 047301 (2013).
[31] B. Singh and J. Chen, Nucl. Data Sheets **116**, 1 (2014).
[32] A. Ozawa *et al.*, Prog. Theor. Exp. Phys. **2012**, 03C009 (2012).